

## ORIGINAL ARTICLE

# Bridging Sunitinib Exposure to Time-to-Tumor Progression in Hepatocellular Carcinoma Patients With Mathematical Modeling of an Angiogenic Biomarker

S Ait-Oudhia<sup>1\*</sup>, DE Mager<sup>2</sup>, V Pokuri<sup>3</sup>, G Tomaszewski<sup>3</sup>, A Groman<sup>3</sup>, P Zagst<sup>3</sup>, G Fetterly<sup>4</sup> and R Iyer<sup>3</sup>

Hepatocellular carcinoma (HCC) is third in cancer-related causes of death worldwide and its treatment is a significant unmet medical need. Sunitinib is a selective tyrosine kinase inhibitor of the angiogenic biomarker: soluble vascular endothelial growth factor receptor-2 (sVEGFR<sub>2</sub>). Sunitinib failed its primary overall survival endpoint in patients with advanced HCC in a phase III trial compared to sorafenib. In the present study, pharmacokinetic-pharmacodynamic modeling was used to link drug-exposure to tumor-growth-inhibition (TGI) and time-to-tumor progression (TTP) through sVEGFR<sub>2</sub> dynamics. The results suggest that 1) active drug concentration (i.e., sunitinib and its metabolite) inhibits the release of sVEGFR<sub>2</sub> and that such inhibition is associated with TGI, and 2) daily sVEGFR<sub>2</sub> exposure is likely a reliable predictor for the TTP in HCC patients. Moreover, the model quantitatively links the dynamics of an angiogenesis biomarker to TTP and accurately predicts observed literature-reported results of placebo treatment.

*CPT Pharmacometrics Syst. Pharmacol.* (2016) 5, 297–304; doi:10.1002/psp4.12084; published online 8 June 2016.

## Study Highlights

### WHAT IS THE CURRENT KNOWLEDGE ON THE TOPIC?

☑ Hepatocellular carcinoma (HCC) is the third deadliest primary neoplasm worldwide. Since HCC is a particularly vascular solid tumor, sunitinib, an antiangiogenic and tyrosine kinase inhibitor of the VEGFR, was investigated in advanced HCC patients.

### WHAT QUESTION DID THIS STUDY ADDRESS?

☑ We utilized a modeling and simulation approach to identify and qualify a plasma biomarker that links active drug exposure (ADE) of sunitinib to its antitumor activity and time-to-tumor progression (TTP)

### WHAT THIS STUDY ADDS TO OUR KNOWLEDGE

☑ Our findings suggest that ADE inhibits sVEGFR<sub>2</sub>, an angiogenesis biomarker, resulting in tumor growth inhibition, and that its daily exposure is a reliable predictor for TTP.

### HOW THIS MIGHT CHANGE DRUG DISCOVERY, DEVELOPMENT, AND/OR THERAPEUTICS

☑ Our model constitutes a rational tool to determine an optimal timepoint for the assessment of angiogenesis in HCC patients based on sVEGFR<sub>2</sub> dynamics and link it to TTP. This model may be applied to other antiangiogenic drugs.

Hepatocellular carcinoma (HCC) is ranked as the sixth most common cancer in the world and the third most common cause of cancer-related deaths worldwide.<sup>1</sup> The global geographical incidence of HCC is wide and variable, with the highest incidence rates (>80%) occurring in the developing countries of Asia and Africa, and an increasing annual incidence in North America and Europe.<sup>2,3</sup> Incidence rates of HCC among men are more frequent than among women, and the leading risk-factors for this disease are hepatitis B and C, alcohol cirrhosis, and nonalcoholic steatohepatitis.<sup>4</sup> The prognosis for patients with advanced HCC is poor, and the estimated 5-year survival rate for untreated symptomatic HCC is less than 5%.<sup>5</sup> Generally, surgical resection, liver transplantation, and percutaneous ablation are the only curative treatments for patients with early stage HCC.<sup>6</sup> However, ~70% of patients are ineligible for curative surgery due to

unresectable or metastatic disease at diagnosis.<sup>7</sup> These patients can only be offered palliative care, with cytotoxic agents contributing a marginal benefit.<sup>8</sup>

Angiogenesis is a pathophysiological process whereby new blood vessels are formed from preexisting capillaries, resulting in an excessive and abnormal vasculature, which contributes to the progression of solid tumors.<sup>9</sup> The role of angiogenesis in HCC development and metastasis is well established, with upregulation of several proangiogenic factors, including: vascular endothelial growth factor-A (VEGF-A), VEGF-D, and platelet-derived endothelial growth factor (PDGF), as well as their corresponding tyrosine kinase receptors VEGFR-1, -2, -3, soluble VEGFR<sub>2</sub> (sVEGFR<sub>2</sub>), and PDGFR. These increased factors promote the pathogenesis, proliferation, and invasiveness of HCC.<sup>10,11</sup> Serum and tissue concentrations of VEGF have significant

<sup>1</sup>Center for Pharmacometrics and Systems Pharmacology, Department of Pharmaceutics, College of Pharmacy, University of Florida, Orlando, Florida, USA; <sup>2</sup>Department of Pharmaceutical Sciences, University at Buffalo, State University of New York, Buffalo, New York, USA; <sup>3</sup>Department of Medical Oncology, Roswell Park Cancer Institute, Buffalo, New York, USA; <sup>4</sup>Clinical Pharmacology and Regulatory Affairs, Buffalo, New York, USA. \*Correspondence: S Ait-Oudhia ([sihem.bihorel@cop.ufl.edu](mailto:sihem.bihorel@cop.ufl.edu))

predictive capacity for projecting overall survival (OS) in HCC and may be useful for defining its prognosis.<sup>12–14</sup>

Sunitinib malate (Sutent) is an oral, multitargeted tyrosine kinase inhibitor with antiangiogenic and antiproliferative cell activities. It is primarily converted by cytochrome P450 3A4 into an active metabolite (SU12662).<sup>15</sup> This metabolite was shown to be equipotent to the parent drug in biochemical tyrosine kinase and cellular proliferation assays towards VEGFR.<sup>16,17</sup> Sunitinib selectively binds and inhibits VEGFRs, PDGFRs, and other growth factors.<sup>18–21</sup> It is presently approved for the treatment of renal cell carcinoma (RCC) and imatinib-resistant gastrointestinal stromal tumor (GIST) at a dose of 50 mg daily over 4 weeks, followed by a 2-week rest period, in repeated 6-week treatment cycles.<sup>22</sup> However, at this dose hematological toxicities are the most frequently observed adverse effects.<sup>15</sup> In a phase III trial, sunitinib efficacy and safety were compared to sorafenib in HCC patients, and sunitinib failed its primary OS endpoint and was associated with more frequent toxicities than sorafenib,<sup>23</sup> leading to its withdrawal from this indication.<sup>23</sup> In the present study, an exposure–response modeling framework for sunitinib in HCC was developed, whereby the angiogenesis biomarker dynamics (i.e., sVEGFR<sub>2</sub>) played a pivotal role in relating the active drug exposure to its antitumor activity and to the time-to-tumor progression (TTP).

## METHODS

### Patients, treatments, and measurements

**Patients and study design.** This study was approved by the Roswell Park Institute Institutional Review Board, and all patients gave written informed consent prior to participation. Eligibility criteria included disease characteristics such as 1) confirmed HCC with 1–4 lesions and involvement of one or both liver lobes; 2) performance Eastern Cooperative Oncology Group (ECOG) of 0, 1, or 2; and 3) a life-expectancy of at least 12 weeks. Patients who had chemo- or radiotherapy 4 weeks prior to the start of the study or a prior liver transplantation were excluded. The study was a single-arm open-label phase II pilot study. Patients received 37.5 mg of sunitinib orally once daily (q.d.) on Days 1–7 prior to transarterial chemoembolization (TACE) with doxorubicin (30 mg) on Day 8. Sunitinib was restarted on Day 15 and continued up to Day 35 followed by a 2-week break. Subsequent cycles were sunitinib for 4 weeks on and 2 weeks off and repeated every 6 weeks in the absence of disease progression or unacceptable toxicity. In patients without contraindication to having repeated magnetic resonance imaging (MRI), a dynamic contrast-enhanced (DCE)-MRI was performed before the start of drug treatment, on Day 8 before TACE, on Day 10 (48 hours after TACE), and on Day 35. Blood samples for the assessment of sunitinib and SU12662 pharmacokinetics (PK) were drawn 24 hours postdosing on days 8, 10, and 35. sVEGFR<sub>2</sub> plasma concentrations were determined at identical sampling times as for the PK. The demographic characteristics of the HCC patients enrolled in the study are summarized in **Supplementary Table S1** and their hematological toxicities are summarized in **Supplementary Table S2**.

**Assays for sunitinib, SU12662, and sVEGFR<sub>2</sub> plasma concentrations.** A liquid chromatography-tandem mass spectrometry assay was used for the assessment of plasma concentrations of sunitinib and its active metabolite as previously described.<sup>17,24,25</sup> The lower limits of detection were 0.099 and 0.088 ng/mL for sunitinib and SU12662. Plasma concentrations of sVEGFR<sub>2</sub> were determined using an enzyme-linked immunosorbent assay kit, following the manufacturer's instructions (eBioScience, San Diego, CA), with a lower limit of detection of 7 pg/mL.

**Tumor volume measurements.** In this study, DCE-MRI was performed in all available patients ( $n = 8$ ) to determine tumor volumes (mm<sup>3</sup>) on Days 8, 10, and 35 as well as at baseline. DCE-MRI also facilitates the determination of the volume transfer constant parameter ( $K_{trans}$ ) via modeling blood and tumor growth data using the Tofts model.<sup>26,27</sup> A reduction in  $K_{trans}$  was associated with a reduction in tumor vascular permeability, perfusion, and growth following the treatment of mice bearing PC-3 human prostate adenocarcinomas with a VEGF receptor-2 tyrosine kinase inhibitor.<sup>28</sup>

**Time-to-tumor progression and overall survival monitoring.** All patients ( $n = 16$ ) were monitored for TTP, and the RECIST criterion for the TTP event was defined as an increase in tumor diameter of at least 20% from its baseline.<sup>29</sup> TTP was reported as probabilities using Kaplan–Meier plots generated in Prism (GraphPad Software, San Diego, CA).

### Model development

**PK modeling of sunitinib and SU12662.** Previously published PK models for the drug (D) and its active metabolite (M) were employed.<sup>30</sup> Briefly, the models each consisted of a two-compartment model with linear elimination from the central compartment ( $CL_D/F_{central}$ ,  $CL_M/F_{central}$ ) and a first-order absorption ( $ka_D$ ,  $ka_M$ ) from the gastrointestinal tract. The fraction of drug metabolized into the active metabolite (SU12662) was fixed ( $f_M = 0.21$ ).<sup>30</sup> The pharmacological activity of sunitinib is attributed to both sunitinib and its equipotent active metabolite.<sup>15–17</sup> Therefore, the active free (i.e., unbound to plasma proteins) molar drug concentration ( $AC_{ub}$ ) was derived as the sum of the unbound molar concentrations of D and M:  $AC_{ub} = C_{ub,D} + C_{ub,M}$ , in which  $C_{ub,D} = (1 - f_{b,D}) \cdot C_D$  and  $C_{ub,M} = (1 - f_{b,M}) \cdot C_M$ , with  $f_{b,D} = 0.9$  and  $f_{b,M} = 0.95$  representing the bound fraction to plasma protein for D and M.<sup>15–17</sup>

**Model equations for sunitinib and SU12662 pharmacokinetics.** The corresponding differential equations for the parent drug (sunitinib) and its active metabolite (SU12662) are:

$$\frac{dA1_D}{dt} = -ka_D \cdot A1_D \quad (1)$$

$$\frac{dA2_D}{dt} = ka_D \cdot A1_D - \left(\frac{CL_D}{V1_D}\right) \cdot A2_D - \left(\frac{Q_D}{V1_D}\right) \cdot A2_D + \left(\frac{Q_D}{V2_D}\right) \cdot A3_D \quad (2)$$

$$\frac{dA_{3D}}{dt} = \left(\frac{Q_D}{V_{1D}}\right) \cdot A_{2D} - \left(\frac{Q_D}{V_{2D}}\right) \cdot A_{3D} \quad (3)$$

with  $A_{1D}(0) = Dose$ ,  $A_{2D}(0)$  and  $A_{3D}(0) = 0$ , and plasma sunitinib concentrations are defined as:  $C_D = \frac{A_{2D}}{V_{2D}}$

$$\frac{dA_{1M}}{dt} = -ka_M \cdot A_{1M} - \left(\frac{CL_M \cdot dt}{V_{1M}}\right) \cdot A_{1M} \quad (4)$$

$$\frac{dA_{2M}}{dt} = ka_M \cdot A_{1M} - \left(\frac{CL_M \cdot dt}{V_{1M}}\right) \cdot A_{2M} - \left(\frac{Q_D}{V_{1M}}\right) \cdot A_{2D} + \left(\frac{Q_D}{V_{2M}}\right) \cdot A_{3D} \quad (5)$$

$$\frac{dA_{3M}}{dt} = \left(\frac{Q_M}{V_{1M}}\right) \cdot A_{2D} - \left(\frac{Q_M}{V_{2M}}\right) \cdot A_{3M} \quad (6)$$

with  $A_{1M}(0) = f_M \cdot Dose$ , and  $f_M$  is the fraction of SU converted into SU12662 (fixed to 0.21) (30).  $A_{2M}(0)$  and  $A_{3M}(0) = 0$ , and plasma SU12662 concentrations are defined as:  $C_M = \frac{A_{2M}}{V_{2M}}$

**PD modeling of sVEGFR<sub>2</sub> concentrations.** The  $AC_{ub}$  served as a driving force for the suppression of sVEGFR<sub>2</sub> plasma concentrations over time, which was best described with an indirect response model in which  $AC_{ub}$  inhibits the zero-order production rate ( $k_{in}$ ) of sVEGFR<sub>2</sub>:

$$\frac{dsVEGFR_2}{dt} = k_{in} \cdot \left(\frac{1}{(1 + \alpha_{sVEGFR_2} \cdot INH)}\right) - k_{out} \cdot sVEGFR_2 \quad (7)$$

with  $INH = \frac{AC_{ub}}{K_d + AC_{ub}}$ , the equilibrium dissociation constant fixed to 4 ng/mL (31),  $\alpha_{sVEGFR_2}$  is the intrinsic activity, and  $K_{in} = BL_{sVEGFR_2} \cdot k_{out}$ ,  $BL_{sVEGFR_2}$  is the sVEGFR<sub>2</sub> baseline concentration, and  $k_{out}$  is the first-order elimination rate constant of sVEGFR<sub>2</sub> from plasma allowing, which defines its typical half-life  $T_{1/2} = \frac{\ln(2)}{k_{out}}$ .

**PD modeling of the HCC tumor growth inhibition.** The predicted difference in the sVEGFR<sub>2</sub> concentrations from its baseline ( $\Delta sVEGFR_2 = sVEGFR_2(0) - sVEGFR_2(t)$ ) over time was linked to the tumor growth (TG) such as:

$$\frac{dTG}{dt} = k_g \cdot (1 - H(t)) \cdot TG \quad (8)$$

with the initial condition being the measured tumor volume at baseline ( $TG_0$ ) and  $H(t) = \frac{I_{max} \cdot \Delta sVEGFR_2}{(\Delta sVEGFR_2 + \Delta IC_{50})}$ . The  $I_{max}$  represents the maximum drug inhibitory effect (fixed to 1), and  $\Delta IC_{50}$  is the  $\Delta sVEGFR_2$  concentration producing 50% of  $I_{max}$ . The natural growth of HCC tumors was modeled using a published relationship between the tumor volume doubling time (TVDT) and  $TG_0$ :  $TVDT = 114 \cdot (TG_0)^{0.14} = \frac{\ln(2)}{k_g}$ .<sup>32</sup>

**Time-to-tumor progression modeling.** In order to explore the relationship between the exposure to  $AC_{ub}$  or  $\Delta sVEGFR_2$  and the TTP probability, several covariates were investigated including: 1) the time-course of  $AC_{ub}$ ; 2) the cumulative area under the concentration time-curve ( $AUC_{cum}$ ) of  $AC_{ub}$ , which accounted for the patients dosing history; 3) the daily AUC ( $AUC_{0-24h}$ ) of  $AC_{ub}$ ; 4) the  $AUC_{0-24h}$  of the change in sVEGFR<sub>2</sub> concentrations from baseline ( $\Delta AUC_{0-24h-sVEGFR_2}$ );

and 5) the time-course of the change in sVEGFR<sub>2</sub> concentrations from its baseline ( $\Delta sVEGFR_2$ ). Thus, five competitive models were tested and compared based on the value of their objective functions (OBJF). The superior model was the one producing the smallest OBJF and corresponded to the one using the  $\Delta AUC_{0-24h-sVEGFR_2}$  as a covariate.

The following functions for the hazard ( $h(t)$ ), survival ( $S(t)$ ) or cumulative hazard, and probability density function  $pdf(t)$  were used such as:

$$h(t) = \beta_0 \cdot \exp(\beta_1 \cdot \Delta AUC_{24h-sVEGFR_2}) \quad (9)$$

$$S(t) = \Pr(T > t) = \exp\left(-\int_0^t h(t) dt\right) \quad (10)$$

$$pdf(t) = h(t) \cdot s(t) \quad (11)$$

with TTP given by:  $TTP = \frac{\ln(1.8)}{k_2}$ , which corresponds to the calculated TTP based on the RECIST criteria for disease progression (i.e., radiologic proliferation of 20% in the tumor diameter from its baseline measurement). The tumor is assumed to be spherical, with a volume given by  $V = \frac{1}{6} \cdot \pi \cdot D^3$ .

#### Data analysis

A joint PK model for sunitinib and SU12662 was fitted to their corresponding data. Then, PK parameters were fixed to sequentially model sVEGFR<sub>2</sub> dynamics, tumor growth kinetics, and TTP probabilities. A MAP-Bayesian approach utilizing prior information on the structural models, the parameter estimates, and their distributions was adopted for the modeling of: 1) the PK of drug and metabolite,<sup>30</sup> 2) the sVEGFR<sub>2</sub> concentrations,<sup>33</sup> and 3) the natural growth of HCC tumors.<sup>32</sup> All priors are summarized in **Supplementary Table S1**. All nonlinear mixed-effect modeling and simulations were conducted with MONOLIX 4.3.2.<sup>34</sup> The parameters for a specific subject ( $P_i$ ) were described as:

$$P_i = P_{pop} \cdot \exp(\eta_i) \quad (12)$$

with  $P_{pop}$  as the typical population parameter, and  $\eta_i$  is the symmetrically distributed between-subject variability with a mean of zero and a variance of  $\omega^2$ . The residual variability, interpreted as the difference between the observed measurements ( $C_{obs}$ ) and model predicted values ( $C_{pred}$ ), was characterized by proportional models (Eq. 13) for sunitinib, SU12662, and sVEGFR<sub>2</sub> concentrations and by an additive model (Eq. 2) for the TGI:

$$C_{obs} = V_{pred} \cdot (1 + \varepsilon_{prop}) \quad (13)$$

$$C_{obs} = C_{pred} \cdot + \varepsilon_{add} \quad (14)$$

with  $\varepsilon_{prop}$  and  $\varepsilon_{add}$  as zero-mean normally distributed variables and variances of  $\sigma_{prop}^2$  and  $\sigma_{add}^2$ .

The effects of available covariates, including body weight, age, gender, and the blood-to-tumor permeability parameter  $K_{trans}$ , were tested for explaining the variability of model parameters controlling the drug and metabolite PK, sVEGFR<sub>2</sub> concentrations, and TGI kinetics. Only  $K_{trans}$  was a statistically significant covariate on the parameter  $\Delta IC_{50}$ , such that  $\Delta IC_{50,i} = \Delta IC_{50,pop} \cdot \left(\frac{K_{trans}}{\text{Median } K_{trans}}\right)^\gamma$ . The final model

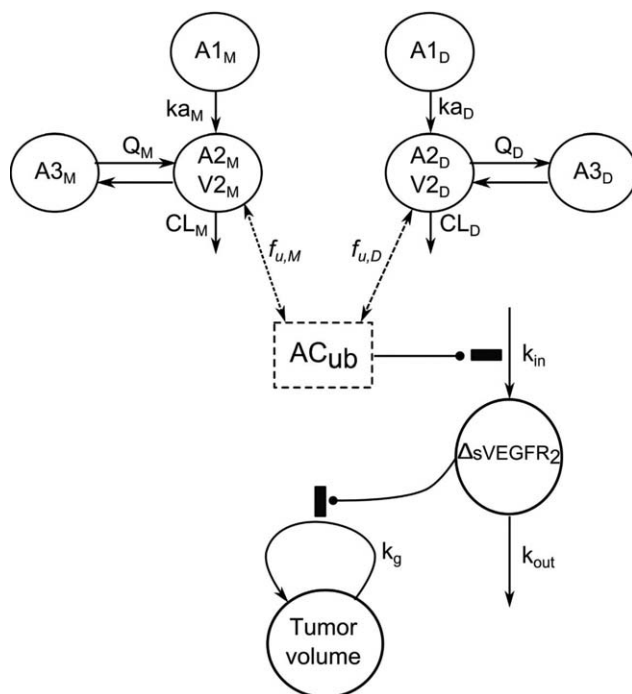


**Figure 1** Pharmacokinetic/pharmacodynamic model for sunitinib and SU12662. Drug (D) and metabolite (M) were described with two-compartment models including linear elimination ( $CL_D$ ,  $CL_M$ ) and first-order absorption from the gastrointestinal tract ( $ka_D$ ,  $ka_M$ ). The fraction of drug metabolized into SU12662 was fixed ( $f_M = 0.21$ ). The active unbound concentration,  $AC_{ub} = f_{ub,D} \cdot CD + f_{ub,M} \cdot CM$ , with  $f_{ub,D}$  and  $f_{ub,M}$  as the free fractions of drug and metabolite, inhibits sVEGFR<sub>2</sub> production, which was captured with an indirect response model with a zero-order production rate constant ( $k_{in}$ ) and a first-order removal rate constant ( $k_{out}$ ). The difference of sVEGFR<sub>2</sub> from its baseline concentration ( $\Delta sVEGFR_2$ ) inhibits the growth rate constant ( $k_g$ ) controlling HCC tumor progression. The symbols are defined in the Methods.

was selected based on the smallest numerical value of the OBF and also the graphical goodness-of-fit plots, including NPDE shown in **Supplementary Figures S5-S7**.

**Calculation of odds ratio.** The odds ratio is calculated with the following equation:  $OR = \exp(\beta_1) = 1.03$ , and can be interpreted as the hazard of experiencing TTP = 3% for every increase in one unit of sVegfR<sub>2</sub> AUC<sub>24h</sub> (i.e., AUC<sub>24h</sub> = 1 μg.h/L). Similarly, if sVegfR<sub>2</sub> AUC<sub>24h</sub> increases by 10 μg.h/L, then the odds increases by  $OR = \exp(10 \cdot \beta_1) = 1.35$ . The 95% confidence interval (CI) for the odds ratio can be calculated as:  $[e^{\beta_1 - 1.96 \cdot SE(\beta_1)}, e^{\beta_1 + 1.96 \cdot SE(\beta_1)}]$  and is equal to [1.01, 1.05].

**Calculation of EL<sub>50</sub>.** EL<sub>50</sub> is the effective level of sVegfR<sub>2</sub> AUC<sub>24h</sub> that predicts 50% of the probability of TTP to occur. It is calculated with the following equation:  $EL_{50} = \frac{\beta_0}{\beta_1}$ , which equals 14.9 μg.h/L and was comprised in the range of sVegfR<sub>2</sub> AUC<sub>24h</sub> (min, max) = (5.034, 147.4) μg.h/L.

## RESULTS

**Figure 1** depicts the schematic representation of the final model linking drug and metabolite exposures to the changes in plasma concentrations of sVEGFR<sub>2</sub> and the inhibition of the HCC expansion. Individual model fittings and goodness of fit plots for SU, SU12662, sVEGFR<sub>2</sub>, and TGI are shown in **Supplementary Figures S1-7**.

### Pharmacokinetic and pharmacodynamic modeling

Sunitinib and SU12662 concentrations were modeled concurrently. For each, the final model included a central, a peripheral, and an absorption compartment. The absorption was characterized as a first-order process, and the disposition was captured with a linear clearance. No covariate effects were identified for the PK parameters. The clearances and volumes of distribution (central and peripheral) were apparent values, and the final parameter estimates are summarized in **Table 1**. The shrinkage values on the parameters are summarized in **Supplementary Table S2**.

Owing to lack of data in the absorption and distribution phases of drug and metabolite, the typical or mean first-order absorption rate constants, the intercompartmental clearances, and peripheral volumes of the distribution were all fixed to values extracted from the literature<sup>30</sup> (**Table 1**). On the contrary, trough concentrations facilitated the estimation of the remaining parameters (i.e., central volume of distribution and linear disposition) by means of prior information on the estimates and distributions of these parameters.<sup>30</sup> The model captured adequately the central tendency of the observed concentrations for sunitinib and SU12662 as depicted in the visual predictive check (VPC) graphs (**Figure 2a,b**).

### Biomarker dynamics

Following sunitinib treatment, the observed plasma concentrations of sVEGFR<sub>2</sub> in HCC patients gradually decreased over time from a mean baseline value of 15.7 μg/L to nearly fall into the range of healthy subjects plasma concentrations 5.5–10 μg/L.<sup>35,36</sup> The proposed model described very well the temporal changes in the dynamics of this biomarker (**Figure 2c**), where the simulated median captures the trend in sVEGFR<sub>2</sub> concentrations, and the predicted 95% CI covers the majority of the data. The potency of  $AC_{ub}$  was estimated at  $0.77 (\mu\text{g/L})^{-1}$ . Owing to the limited data for sVEGFR<sub>2</sub>, the parameter  $k_{out}$  was fixed and priors on the remaining parameters were used.<sup>33</sup> All parameters were obtained with good precision and no significant covariates were identified.

### Tumor growth inhibition model

Only 8/16 patients were qualified to receive DCE-MRI throughout the clinical trial. There was no placebo arm in this trial; therefore, the natural growth of HCC tumors was obtained from a published report.<sup>32</sup> This allowed for the identification of the growth rate parameter ( $k_g$ ), depending on TG<sub>0</sub> such as  $TVDT = \frac{Ln(2)}{k_g}$ , with  $TVDT = 114 \cdot (TG_0)^{0.14}$ , thus  $k_g = \frac{Ln(2)}{114 \cdot TG_0^{0.14}}$ . The cytostatic effects of the parent drug and its active metabolite were integrated into the TGI model via the sVEGFR<sub>2</sub> dynamics.<sup>37</sup> The developed TGI model accurately described the observed tumor volumes under sunitinib exposure as shown by the VPC (**Figure 2d**). All parameters

**Table 1** Pharmacokinetic parameter estimates for sunitinib and SU12662

Parameter (unit)	Definition	Estimate (RSE%)	Between subject variability, %CV (RSE%)
<i>Sunitinib</i>			
$V_{1D}/F_{\text{central}}$ (L)	Central volume of distribution	1,777 (39)	44.7 (13) <sup>a</sup>
$CL_D/F_{\text{central}}$ (L/h)	Linear clearance	30.3 (14)	37.9 (8.8) <sup>a</sup>
$ka_D^a$ (1/h)	First-order absorption rate constant	0.195 (6.8)	81.2 (13) <sup>a</sup>
$Q_D/F_{\text{peripheral}}^a$ (L/h)	Intercompartmental clearance	6.37 (18)	NA
$V_{2D}/F_{\text{peripheral}}^a$ (L)	Peripheral volume of distribution	588 (8.7)	NA
$\epsilon_{\text{sunitinib}}$	Proportional error coefficient	0.31 (16)	NA
<i>SU12662</i>			
$V_{1M}/F_{\text{central}}$ (L)	Central volume of distribution	1840 (25)	65.1 (8.7) <sup>a</sup>
$CL_M/F_{\text{central}}$ (L/h)	Linear clearance	19.72 (19)	52.2 (8.5) <sup>a</sup>
$ka_M^a$ (1/h)	First-order absorption rate constant	0.487 (6.6)	89.1 (13)
$Q_M/F_{\text{peripheral}}^a$ (L/h)	Intercompartmental clearance	27.7 (26)	NA
$V_{2M}/F_{\text{peripheral}}^a$ (L)	Peripheral volume of distribution	345 (22)	NA
$\epsilon_{\text{metabolite}}$	Proportional error coefficient	0.16 (21)	NA

<sup>a</sup>Fixed from Ref. 30.  $F_{\text{central}}$  and  $F_{\text{peripheral}}$  are the drug and metabolite bioavailabilities in central and peripheral compartments. RSE, residual standard error; CV, coefficient of variation.

were precisely estimated (**Table 2**). The potency of  $\Delta s\text{VEGFR}_2$  to inhibit HCC growth was  $\Delta IC_{50} = 1.83 \mu\text{g/L}$ . The permeability parameter,  $K_{\text{trans}}$ , was identified as a significant covariate on  $\Delta IC_{50}$ . Model simulation of the unperturbed HCC tumor growth from Ref. 32 is shown in **Figure 2d**.

#### Time-to-tumor progression probabilities analysis

Kaplan–Meier representations of the observed TTP probabilities is displayed in **Figure 3**, where the median observed TTP is 7 months. The developed TTP model predicted a median TTP of 7.4 months. To interpret the fitted parameters from the TTP model, two factors were derived: 1) the odds ratio (OR), which is defined as the hazard of experiencing an event (i.e., disease progression), calculated with  $OR = \exp(\beta_1)$ , and was estimated at 1.03, and 2) the effective level ( $EL_{50}$ ), which is defined as the value of  $\Delta AUC_{24h}$  for  $s\text{VEGFR}_2$  that is responsible for 50% probability of experiencing a TTP. It was calculated according to:  $EL_{50} = \frac{b_0}{\beta_1}$  and was estimated at  $14.9 \mu\text{g/L}$ . The OR translates as an increase of 3% in the risk of disease progression to occur for every 1 h. $\mu\text{g/L}$  increase of  $s\text{VEGFR}_2$  exposure. In other words, an increase of 1.35 in the risk of the disease progression will occur for every 100 h. $\mu\text{g/L}$  of  $s\text{VEGFR}_2$  exposure, and the  $EL_{50}$  is included in the range of  $\Delta AUC_{24h}$  for  $s\text{VEGFR}_2$  (min, max) at (5.034, 147.4) h. $\mu\text{g/L}$ .

## DISCUSSION

Unlike for cytotoxic chemotherapeutics, targeted cancer therapies, such as angiogenesis inhibitors, may achieve therapeutic concentrations well below those associated with toxicities.<sup>38</sup> For this reason, it is necessary to identify biomarkers for angiogenesis that accurately reflect the effect of a drug on its target and predict response to treatment.<sup>39</sup> Current angiogenesis inhibitors, such as sunitinib, are typically cytostatic and are thought to alter vessel structure instead of resulting in direct tumor kill. Therefore, investigators are aggressively pursuing suitable markers of antiangiogenic modulation of tumor

vasculature. This search has been challenging due to variations of tumor vasculature between tumor types, tumor histologies, tumor size, and degree of differentiation.<sup>40</sup>

The accessibility of measurable circulating angiogenic biomarkers makes them more attractive than tissue biopsies. For example, plasma  $s\text{VEGFR}_2$  has previously been identified as a biomarker of angiogenesis in GIST,<sup>41</sup> in which its plasma concentrations were consistently modulated by sunitinib treatment; however, there was no clear correlation with clinical response. Similarly, patients with metastatic breast cancer, as well as patients with neuroendocrine tumors treated with sunitinib, also showed a decrease in plasma  $s\text{VEGFR}_2$  concentrations.<sup>42,43</sup> In line with these findings, our analysis employed plasma  $s\text{VEGFR}_2$  concentrations as a bridge between the plasma concentrations of sunitinib and its active metabolite and their cytostatic effects on HCC tumors in this patients population. The working hypothesis is that sunitinib acts by suppressing the release of  $s\text{VEGFR}_2$  from endothelial cells into the circulation. This mechanism was integrated in our model, and previously by others,<sup>33,44,45</sup> with  $AC_{\text{ub}}$ , derived based on *in vitro* data<sup>15–17</sup> and kinase inhibition,<sup>31</sup> as a driver to the inhibitory effect on biomarker expression. The estimated drug potency on  $s\text{VEGFR}_2$  inhibition was  $0.77 (\mu\text{g/L})^{-1}$ , which is consistent with previous results from modeling sunitinib effects on  $s\text{VEGFR}_2$  response in healthy subjects.<sup>33</sup> In contrast, the baseline  $s\text{VEGFR}_2$  plasma concentration was estimated to be twice greater in HCC patients than healthy subjects (18.3 vs. 5–10  $\mu\text{g/L}$ ).<sup>33,36</sup> This finding agrees well with *in vitro* data showing the overexpression of VEGF mRNA in several HCC cell lines,<sup>46</sup> as well as the established prognostic angiogenic role of VEGF in HCC.<sup>12–14</sup>

Throughout the duration of this trial under sunitinib treatment, HCC tumor volumes remained relatively unchanged compared to their baseline values, which made it difficult to identify the natural growth rate constant (kg) from the observed data, especially without a placebo arm in the trial. To overcome this limitation, we used a published

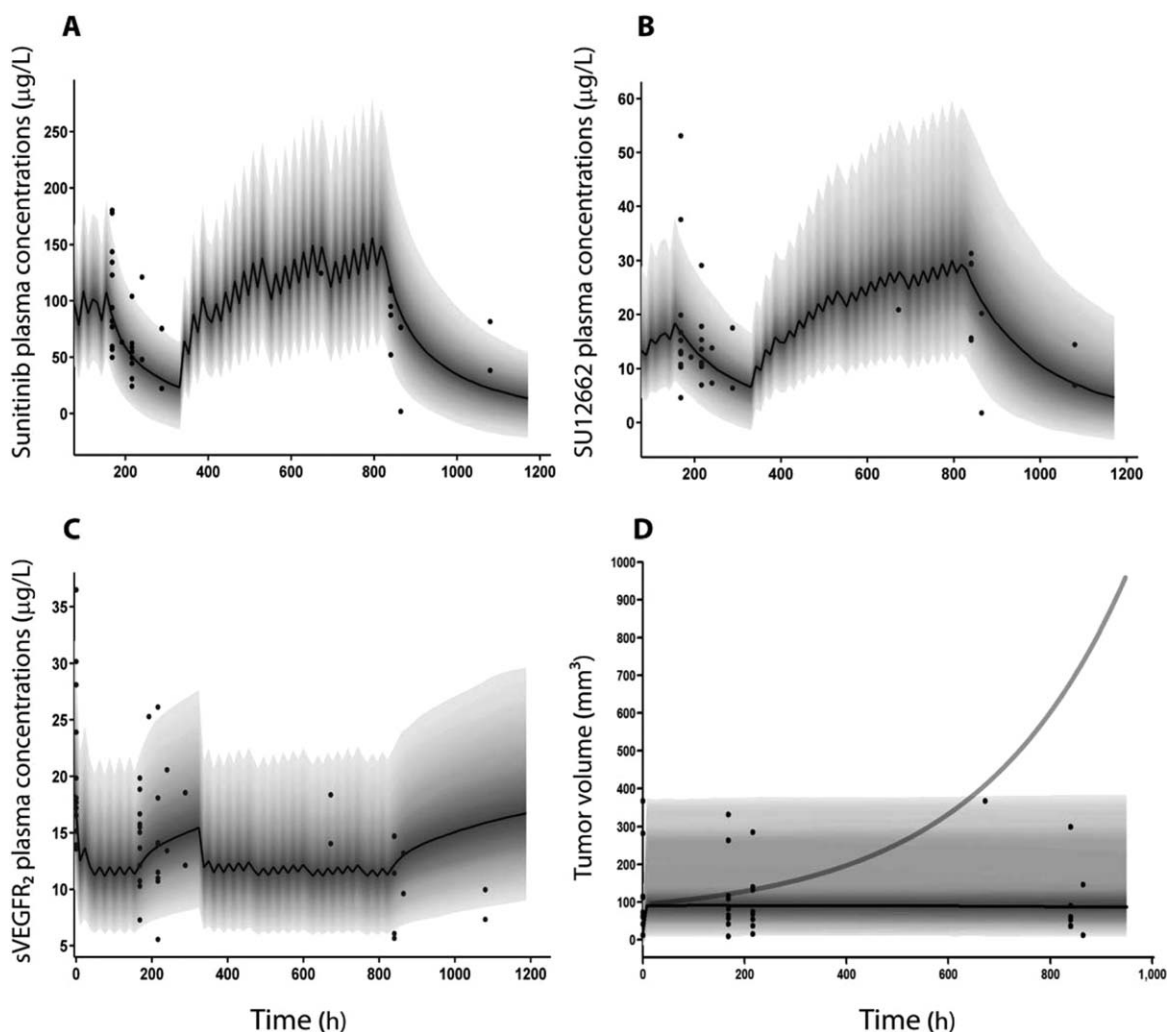


**Figure 2** Visual predictive check (VPC) plots vs. time for (a) sunitinib plasma concentrations, (b) SU12662 plasma concentrations, (c) sVEGFR2 plasma concentrations, and (d) tumor volume kinetics. Solid circles represent the observed data. The gray area identifies the 5th and 95th percentiles of the predicted data, and dark solid lines represent the 50th percentile (median) of the predicted data. The gray solid line in (d) represents a model simulation of the trajectory of the tumor growth in placebo-treated patients. The confidence interval includes the majority of the data and the median is centrally located, although the number of observations outside the predicted 90% confidence interval is slightly above the expected 10%. These VPCs show no specific deviation of predicted vs. observed data, which qualifies the model as being structurally sound and supports the veracity of the estimated parameter values and concentrations.

relationship for the natural growth of HCC tumors, and it was assumed that patients involved in the current trial would follow a similar temporal trajectory of HCC tumor progression.<sup>32</sup> However, we acknowledge that this assumption might not be completely valid. The use of  $\Delta$ sVEGFR<sub>2</sub> dynamics as an indirect driver behind the cytostatic effect of the drug correlates well with the role of angiogenesis in the progression of cancer<sup>47</sup> and has been utilized as an indirect driver for sunitinib cytostatic effects on the gastrointestinal and stomach tumor growth.<sup>44,45</sup> The fitted  $\Delta$ sVEGFR<sub>2</sub> potency (1.83 µg/L) is comparable to the *in vitro* measured IC<sub>50</sub> of sunitinib for cells expressing VEGFR<sub>2</sub> (10 nM or 1.6 µg/L),<sup>36,48</sup> supporting the model in describing HCC growth inhibition kinetics. No particular temporal trend was observed for the permeability parameter  $K_{trans}$ . However, its influence as a covariate on the potency of sVEGFR<sub>2</sub> validates its use as a marker for the

control of vessel leakiness, and suggests it might represent a determinant of HCC response to sunitinib.

The patients included in this trial exhibited a median observed TTP of 8 months (95% CI 7.2–9.6). This clinical endpoint for sunitinib treatment is longer than previously reported for a higher dose of sunitinib (50 mg q.d. in 4/2 weeks schedule), with a median value of 5.3 months (95% CI = 2.7–7.9).<sup>49</sup> Several hypotheses may explain the moderate but greater benefit observed in our study, such as: 1) differences in patient HCC baseline characteristics between trials, 2) the absence of hematological toxicities (see **Supplementary Table S2**), and 3) the inclusion of TACE therapy with doxorubicin. As TACE therapy was administered to all patients, and because of unavailability of TACE therapy data (i.e., DOX treatment), the final TTP model did not include TACE therapy. Our primary goal from modeling TTP was to screen for a prognostic covariate that

**Table 2** Pharmacodynamic parameters for VEGFR<sub>2</sub> concentrations, tumor growth kinetics, and time-to-tumor progression

Parameter (unit)	Definition	Estimate (RSE%)	Between subject variability, %CV (RSE%)
<i>VEGFR<sub>2</sub></i>			
$k_{out}$ (1/day) <sup>a</sup>	First-order removal rate constant	0.175 (NA)	67 (66)
$\alpha$ ( $\mu\text{g/L}$ ) <sup>-1</sup>	Slope effect of $AC_{ub}$ on VegfR2	0.77 (14)	21 (12.3)
$R_0$ ( $\mu\text{g/L}$ )	VegfR2 baseline level	18.3 (8)	34.4 (57)
$\varepsilon_{vegfr2}$	Proportional error coefficient	0.26 (14)	NA
<i>Tumor growth</i>			
$\Delta IC_{50}$ ( $\mu\text{g/L}$ )	$\Delta sVEGFR_2$ concentration for 50% of $I_{max}$	1.83 (41)	36 (49)
$\beta$	Power coefficient for $K_{trans}$ covariate	2.12 (49)	NA
$\varepsilon_{TG}$ ( $\text{mm}^3$ )	Additive error coefficient	15.5 (13)	NA
<i>Time-to-tumor progression</i>			
$\beta_0$ ( $\text{month}^{-1}$ )	Baseline hazard	0.448 (6)	NA
$\beta_1$ ( $\text{h} \cdot \mu\text{g/L}$ ) <sup>-1</sup>	Slope for time-to-tumor progression	0.0483 (6)	NA
	Slope hazard $\Delta AUC_{0-24h}$ $sVEGFR_2$	0.03 (33)	NA

Fixed from Ref 33.  $I_{max} = 1$  Fixed. RSE, residual standard error; CV, coefficient of variation.

discriminates patient outcome to sunitinib treatment. The  $\Delta AUC_{24h}$  of  $sVEGFR_2$  concentrations predict well the observed data (Figure 3). Furthermore, the aggressiveness of certain HCC lesions has been linked to high concentrations of VEGF suggesting the ability of VEGF to predict HCC prognosis.<sup>12–14</sup> Moreover, model simulations of TTP profiles in a hypothetical placebo group (Figure 3) predicted the median TTP at 2.5 months, which agrees well with observed data in advanced HCC patients treated with placebo from a phase III trial of sorafenib.<sup>50</sup>

In this analysis, we used  $sVEGFR_2$  as a surrogate biomarker to angiogenesis. For every unit (i.e., 1  $\mu\text{g} \cdot \text{h/L}$ ) of daily  $sVEGFR_2$  exposure, the OR for the hazard of experiencing a tumor progression increases by 3%, and the effective level of  $\Delta AUC_{24h}$  of  $sVEGFR_2$  for predicting 50% probability of TTP to occur was estimated at 14.9  $\mu\text{g} \cdot \text{h/L}$ . As an example, among the patients included in this analy-

sis we identified two who showed a high and a low increase in the OR (5.7% and 1.7% vs. 3%) and their corresponding  $EL_{50}$  for  $sVEGFR_2$  were 121.9 and 6.8  $\mu\text{g} \cdot \text{h/L}$ . Coincidentally, the prognosis for the first patient was very poor, with an observed TTP occurring at only 1.74 months after the start of sunitinib therapy, whereas the second patient showed a better clinical outcome, with a TTP occurring after 8 months. These findings lead to the conclusion that high OR and high  $EL_{50}$  values would be associated with poor HCC prognosis, whereas low OR and low  $EL_{50}$  would be associated with a better clinical outcome. Furthermore, given that the  $EL_{50}$  is the  $\Delta AUC_{24h}$  of  $sVEGFR_2$  that predicts 50% of the probability of TTP to occur, it can be interpreted as a direct predictor of patients' outcome, whereas the OR can be viewed as an indirect predictor to patients' outcome given its indirect relationship to the  $\Delta AUC_{24h}$  of  $sVEGFR_2$  through the parameter  $\beta_1$  (i.e., slope for  $\Delta AUC_{24h}$  of  $sVEGFR_2$ , Eq. 9). These results support the finding that  $\Delta AUC_{24h}$  of  $sVEGFR_2$  concentrations is a reliable predictor for TTP and reinforces the use of the effective levels 50% of  $sVEGFR_2$  and the OR as useful pharmacometric determinants that allow clinicians to anticipate patient prognosis, and hence potentially adjust chemotherapy treatment for a more beneficial clinical outcome.

In summary, a model-based analysis identified the difference in daily  $sVEGFR_2$  exposure from baseline as a reliable covariate to predict the time-to-tumor progression for an antiangiogenic tyrosine kinase inhibitor (sunitinib). It might be possible to identify an optimal timepoint for the assessment of angiogenesis based on daily exposure of  $sVEGFR_2$ , which can be determined and integrated into the final model of TTP. This model may serve as a useful starting point for assessing other antiangiogenic drugs.

**Acknowledgments.** We thank Dr. Robert Straubinger for suggestions and general guidance. We also thank all the patients, clinicians, and staff that were responsible for generating the data used in this study.

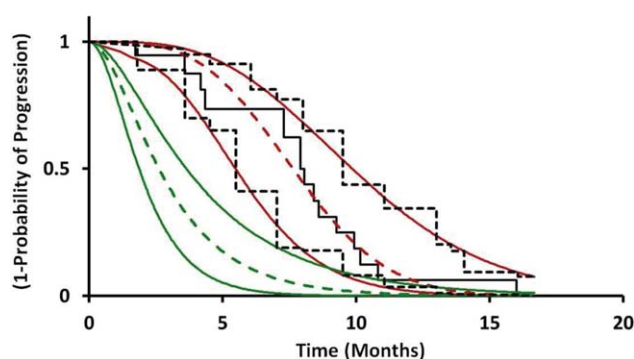


**Figure 3** Model-predicted TTP probabilities in patients with unresectable HCC. The solid black line represents the observed TTP probability. The solid red lines are the 5<sup>th</sup> and 95<sup>th</sup> percentiles of the predicted data, and the red dashed line is the 50<sup>th</sup> percentile (median) of the predicted data in patients treated with sunitinib. Model simulated TTP probability in placebo-treated patients is shown in green, where solid lines represent the 5<sup>th</sup> and 95<sup>th</sup> percentiles and the dashed line is the 50<sup>th</sup> percentile (median).

**Conflict of Interest.** The authors declare no conflicts of interest.

**Author Contributions.** S.A.O., D.E.M., and V.P. wrote the manuscript; V.P. and R.I. designed the research; performed the research; S.A.O. analyzed the data; D.E.M. provided financial support to S.A.O.; G.T., A.G., P.Z., and G.F. contributed new reagents/analytical tools.

1. Parkin, D.M., Bray, F., Ferlay, J. & Pisani, P. Global cancer statistics, 2002. *CA Cancer J. Clin.* **55**, 74–108 (2005).
2. El-Serag, H.B. Epidemiology of hepatocellular carcinoma in USA. *Hepatology* **37**(suppl. 2), S88–94 (2007).
3. El-Serag, H.B. & Rudolph, K.L. Hepatocellular carcinoma: epidemiology and molecular carcinogenesis. *Gastroenterology* **132**, 2557–2576 (2007).
4. El-Serag, H.B. Hepatocellular carcinoma. *N. Engl. J. Med.* **365**, 1118–1127 (2011).
5. El-Serag, H.B. & Mason, A.C. Rising incidence of hepatocellular carcinoma in the United States. *N. Engl. J. Med.* **340**, 745–750 (1999).
6. Forner, A., Llovet, J.M. & Bruix, J. Hepatocellular carcinoma. *Lancet* **379**, 1245–1255 (2012).
7. Llovet, J.M. *et al.* Design and endpoints of clinical trials in hepatocellular carcinoma. *J. Natl. Cancer Inst.* **100**, 698–711 (2008).
8. Zhu, A.X. Systemic therapy of advanced hepatocellular carcinoma: how hopeful should we be? *Oncologist* **11**, 790–800 (2006).
9. Folkman, J. Tumor angiogenesis: therapeutic implications. *N. Engl. J. Med.* **285**, 1182–1186 (1971).
10. Pang, R. & Poon, R.T. Angiogenesis and antiangiogenic therapy in hepatocellular carcinoma. *Cancer Lett.* **242**, 151–167 (2006).
11. Sun, H.C. & Tang, Z.Y. Angiogenesis in hepatocellular carcinoma: the retrospectives and perspectives. *J. Cancer Res. Clin. Oncol.* **130**, 307–319 (2004).
12. Schoenleber, S.J., Kurtz, D.M., Talwalkar, J.A., Roberts, L.R. & Gores, G.J. Prognostic role of vascular endothelial growth factor in hepatocellular carcinoma: systematic review and meta-analysis. *Br. J. Cancer* **100**, 1385–1392 (2009).
13. Li, X.M., Tang, Z.Y., Zhou, G., Lui, Y.K. & Ye, S.L. Significance of vascular endothelial growth factor mRNA expression in invasion and metastasis of hepatocellular carcinoma. *J. Exp. Clin. Cancer Res.* **17**, 13–17 (1998).
14. Kanda, M. *et al.* Correlations of the expression of vascular endothelial growth factor B and its isoforms in hepatocellular carcinoma with clinico-pathological parameters. *J. Surg. Oncol.* **98**, 190–196 (2008).
15. Rini, B.I. Sunitinib. *Expert Opin. Pharmacother.* **8**, 2359–2369 (2007).
16. Pfizer. Sutent (sunitinib) capsules prescribing information. <[http://www.accessdata.fda.gov/drugsatfda\\_docs/label/2012/021938s021s022s023lbl.pdf](http://www.accessdata.fda.gov/drugsatfda_docs/label/2012/021938s021s022s023lbl.pdf)>.
17. Faivre, S. *et al.* Safety, pharmacokinetic, and antitumor activity of SU11248, a novel oral multitarget tyrosine kinase inhibitor, in patients with cancer. *J. Clin. Oncol.* **24**, 25–35 (2006).
18. Kim, D.W. *et al.* An orally administered multitarget tyrosine kinase inhibitor, SU11248, is a novel potent inhibitor of thyroid oncogenic RET/papillary thyroid cancer kinases. *J. Clin. Endocrinol. Metab.* **91**, 4070–4076 (2006).
19. O'Farrell, A.M. *et al.* An innovative phase I clinical study demonstrates inhibition of FLT3 phosphorylation by SU11248 in acute myeloid leukemia patients. *Clin. Cancer Res.* **9**, 5465–5476 (2003).
20. Murray, L.J. *et al.* SU11248 inhibits tumor growth and CSF-1R-dependent osteolysis in an experimental breast cancer bone metastasis model. *Clin. Exp. Metastasis* **20**, 757–766 (2003).
21. Abrams, T.J., Lee, L.B., Murray, L.J., Pryer, N.K. & Cherrington, J.M. SU11248 inhibits KIT and platelet-derived growth factor receptor beta in preclinical models of human small cell lung cancer. *Mol. Cancer Ther.* **2**, 471–478 (2003).
22. Sutent prescribing information. <[http://www.cigna.com/customer\\_care/healthcare\\_professional/coverage\\_positions/pharmacy/ph\\_6111\\_coveragepositioncriteria\\_sunitinib\\_sutent.pdf](http://www.cigna.com/customer_care/healthcare_professional/coverage_positions/pharmacy/ph_6111_coveragepositioncriteria_sunitinib_sutent.pdf)>
23. Cheng, A. *et al.* Phase III trial of sunitinib (Su) vs. sorafenib (So) in advanced hepatocellular carcinoma (HCC). *J. Clin. Oncol.* **29**(suppl. Abstr 4000) (2011).
24. Bello, C.L. *et al.* Effect of food on the pharmacokinetics of sunitinib malate (SU11248), a multi-targeted receptor tyrosine kinase inhibitor: results from a phase I study in healthy subjects. *Anticancer Drugs* **17**, 353–358 (2006).
25. O'Farrell, A.M. *et al.* SU11248 is a novel FLT3 tyrosine kinase inhibitor with potent activity in vitro and in vivo. *Blood* **101**, 3597–3605 (2003).
26. Yuh, W.T. An exciting and challenging role for the advanced contrast MR imaging. *J. Magn. Reson. Imaging* **10**, 221–222 (1999).
27. Padhani, A.R. Dynamic contrast-enhanced MRI in clinical oncology: current status and future directions. *J. Magn. Reson. Imaging* **16**, 407–422 (2002).

28. Checkley, D., Tessier, J.J., Kendrew, J., Waterton, J.C. & Wedge, S.R. Use of dynamic contrast-enhanced MRI to evaluate acute treatment with ZD6474, a VEGF signalling inhibitor, in PC-3 prostate tumours. *Br. J. Cancer* **89**, 1889–1895 (2003).
29. Eisenhauer, E.A. *et al.* New response evaluation criteria in solid tumours: revised RECIST guideline (version 1.1). *Eur. J. Cancer* **45**, 228–247 (2009).
30. Houk, B.E., Bello, C.L., Kang, D. & Amantea, M. A population pharmacokinetic meta-analysis of sunitinib malate (SU11248) and its primary metabolite (SU12662) in healthy volunteers and oncology patients. *Clin. Cancer Res.* **15**, 2497–2506 (2009).
31. Mendel, D.B. *et al.* In vivo antitumor activity of SU11248, a novel tyrosine kinase inhibitor targeting vascular endothelial growth factor and platelet-derived growth factor receptors: determination of a pharmacokinetic/pharmacodynamic relationship. *Clin. Cancer Res.* **9**, 327–337 (2003).
32. Taouli, B. *et al.* Growth rate of hepatocellular carcinoma: evaluation with serial computed tomography or magnetic resonance imaging. *J. Comput. Assist. Tomogr.* **29**, 425–429 (2005).
33. Lindauer, A. *et al.* Pharmacokinetic/pharmacodynamic modeling of biomarker response to sunitinib in healthy volunteers. *Clin. Pharmacol. Ther.* **87**, 601–608 (2010).
34. The Monolix software. <<http://www.lixoft.com/monolix/documentation/>>.
35. Jantus-Lewintre, E. *et al.* Combined VEGF-A and VEGFR-2 concentrations in plasma: diagnostic and prognostic implications in patients with advanced NSCLC. *Lung Cancer* **74**, 326–331 (2011).
36. Ebos, J.M. *et al.* A naturally occurring soluble form of vascular endothelial growth factor receptor 2 detected in mouse and human plasma. *Mol. Cancer Res.* **2**, 315–326 (2004).
37. Garrett, E.R. Drug action and assay by microbial kinetics. *Prog. Drug Res.* **15**, 271–352 (1971).
38. Kummar, S. *et al.* Compressing drug development timelines in oncology using phase '0' trials. *Nat. Rev. Cancer* **7**, 131–139 (2007).
39. Jubb, A.M., Oates, A.J., Holden, S. & Koeppen, H. Predicting benefit from anti-angiogenic agents in malignancy. *Nat. Rev. Cancer* **6**, 626–635 (2006).
40. Sessa, C., Guibal, A., Del Conte, G. & Ruegg, C. Biomarkers of angiogenesis for the development of antiangiogenic therapies in oncology: tools or decorations? *Nat. Clin. Pract. Oncol.* **5**, 378–391 (2008).
41. Norden-Zfoni, A. *et al.* Blood-based biomarkers of SU11248 activity and clinical outcome in patients with metastatic imatinib-resistant gastrointestinal stromal tumor. *Clin. Cancer Res.* **13**, 2643–2650 (2007).
42. Bello, C.L. *et al.* Analysis of circulating biomarkers of sunitinib malate in patients with unresectable neuroendocrine tumors (NET): VEGF, IL-8, and soluble VEGF receptors 2 and 3. *J. Clin. Oncol.* **24**(suppl. Abstr 4045), 189s (2006).
43. Deprimo, S.E. *et al.* Effect of treatment with sunitinib malate, a multitargeted tyrosine kinase inhibitor, on circulating plasma levels of VEGF, soluble VEGF receptors 2 and 3, and soluble KIT in patients with metastatic breast cancer. ASCO Annual Meeting Proceedings Abstr 578 (2006).
44. Hansson, E.K. *et al.* PKPD Modeling of VEGF, sVEGFR-2, sVEGFR-3, and sKIT as predictors of tumor dynamics and overall survival following sunitinib treatment in GIST. *CPT: Pharmacometrics Syst. Pharmacol.* **2**, e84 (2013).
45. Hansson, E.K. *et al.* PKPD modeling of predictors for adverse effects and overall survival in sunitinib-treated patients with GIST. *CPT: Pharmacometrics Syst. Pharmacol.* **2**, e85 (2013).
46. Miura, H. *et al.* Increased expression of vascular endothelial growth factor in human hepatocellular carcinoma. *J. Hepatol.* **27**, 854–861 (1997).
47. Weis, S.M. & Cheresh, D.A. Tumor angiogenesis: molecular pathways and therapeutic targets. *Nat. Med.* **17**, 1359–1370 (2011).
48. Roskoski, R., Jr. Sunitinib: a VEGF and PDGF receptor protein kinase and angiogenesis inhibitor. *Biochem. Biophys. Res. Commun.* **356**, 323–328 (2007).
49. Faivre, S. *et al.* Safety and efficacy of sunitinib in patients with advanced hepatocellular carcinoma: an open-label, multicentre, phase II study. *Lancet Oncol.* **10**, 794–800 (2009).
50. Llovet, J.M. *et al.* Sorafenib in advanced hepatocellular carcinoma. *N. Engl. J. Med.* **359**, 378–390 (2008).

© 2016 The Authors CPT: Pharmacometrics & Systems Pharmacology published by Wiley Periodicals, Inc. on behalf of American Society for Clinical Pharmacology and Therapeutics. This is an open access article under the terms of the Creative Commons Attribution-NonCommercial-NoDerivs License, which permits use and distribution in any medium, provided the original work is properly cited, the use is non-commercial and no modifications or adaptations are made.

Supplementary information accompanies this paper on the CPT: Pharmacometrics & Systems Pharmacology website (<http://www.wileyonlinelibrary.com/psp4>)